

Generation of nonclassical states in nonlinear oscillators via Lyapunov controlDu Ran ^{1,2,3} Wu-Jiang Shan,⁴ Zhi-Cheng Shi,^{2,*} Zhen-Biao Yang ² Jie Song,⁵ and Yan Xia^{2,†}¹*School of Electronic Information Engineering, Yangtze Normal University, Chongqing 408100, China*²*Fujian Key Laboratory of Quantum Information and Quantum Optics (Fuzhou University), Fuzhou 350116, China*³*Department of Electrical Engineering Physical Electronics, Tel Aviv University, Ramat Aviv 69978, Israel*⁴*School of General Education, Jiangxi Vocational College of Industry and Engineering, Pingxiang 337055, China*⁵*Department of Physics, Harbin Institute of Technology, Harbin 150001, China*

(Received 18 October 2019; revised 12 July 2020; accepted 17 July 2020; published 5 August 2020)

In this paper, we propose a scheme to generate nonclassical states in a nonlinear oscillator system, such as Fock states, squeezed coherent states, Schrödinger-cat states, etc. These nonclassical states are achieved by directly applying the classical field to the nonlinear oscillator, where the amplitude of the field is customized through a state-based Lyapunov control. For generating Fock states, there is no need to precisely control the operation time. As for the generation of other nonclassical states, we resort to a unitary transformation to design the control field, resulting in the requirement of a specific time. The Wigner function of the generated states shows the nonclassical property and shape that matches well with the target. Numerical simulations suggest that the scheme is robust against the field fluctuations and immune to variations in the initial state. In addition, the time-varying control field can be replaced by a square pulse based on the characteristics of the Lyapunov control, which may reduce the difficulty of the experiment.

DOI: [10.1103/PhysRevA.102.022603](https://doi.org/10.1103/PhysRevA.102.022603)**I. INTRODUCTION**

The generation and manipulation of nonclassical states of the single-mode fields is one of the most important subjects in quantum optics [1]. Among these states, Fock states play an important role in quantum information processing, including in quantum key distribution [2], quantum memory [3], and quantum communication [4]. In addition, superpositions of Fock states, which give rise to new nonclassical features due to their quantum interference, are also of great interest in the field of quantum science. Particularly, the superpositions with a definite phase relationship between Fock states are the most appealing ones, e.g., coherent states [5], Schrödinger-cat states [6], displaced Fock states [7], squeezed states [8], squeezed coherent states [9], etc. These superpositions are the key ingredients for the foundational tests of quantum theory, such as squeezed states enabling high-precision measurement [10] and a Fock-state superposition with the binomial distribution facilitating quantum error correction [11]. Therefore, the generation of Fock states and their superpositions has drawn much attention in recent years [12–16].

Generally, the dynamics of harmonic oscillators can be described by Fock states. However, the generation of such states and their specific superpositions is a nontrivial task, since classical excitations may lead to a thermal state when they are directly applied to an oscillator system. To overcome the difficulties, one always interposes a nonlinear quantum system (such as a two-level atomic system or a spin-1/2 system) to the resonator [17,18]. Then, the classical pulse is

applied to the nonlinear system to create a quantum state that can subsequently be transferred to the resonator. Here, the nonlinear quantum system plays the role of intermediary between the classical microwave source and the resonator. Such a technique has been demonstrated for the preparation of Fock states for an optical cavity with Rydberg atoms [19,20] and for a superconducting resonator with a superconducting phase qubit [21]. Arbitrary superpositions have also been synthesized in this way [22–24]. In addition, controlled hole burning (erasing one or multiple Fock-state in a coherent state) has been realized via resonant [25] and dispersive interaction [26]. The Schrödinger-cat states of a cavity have been generated by dispersively coupling atoms to the cavity mode [27] and observed in the strongly coupled qubit-oscillator circuits [28]. Moreover, the generation of squeezed states has been theoretically investigated [29] and experimentally implemented [30] in superconducting resonators. Notably, the preparation of Fock states and their superpositions sometimes combines the driving nonlinear quantum system with measurements [31,32], adiabatic passage [33,34], and postselection [35].

Recently, there have been attempts to generate the nonclassical states such as Fock states and their superpositions by directly applying a classical field to the oscillator without auxiliary nonlinear driving systems [36]. Periodical Gaussian pulses were forced on the single-mode oscillator, with the degeneracy of the energy-level spacings being avoided through strong Kerr nonlinearities. By setting the parameters to meet a near-resonant condition, the low-lying Fock states and their superpositions were produced. Notably, the periodical driving scheme may have difficulty in producing the high-lying Fock states and the superpositions with a definite phase relationship between Fock states. Although the high-lying Fock states can be realized by adiabatically varying the detuning of the cavity

*szc2014@yeah.net

†xia-208@163.com

and the strength of the field [37], a simple and versatile protocol that can achieve both Fock states and their superpositions is desirable.

In this paper, we propose a feasible scheme to generate nonclassical states in the nonlinear oscillator systems, such as Fock states, superpositions of Fock states, coherent states, squeezed coherent states and Schrödinger-cat states. The scheme is also suitable for the production of other nonclassical states, such as squeezed Fock states, displaced Fock states, etc. Instead of coupling a two-level driving system to the resonator, we directly apply the external classical field to the nonlinear oscillator system, where the strength of the driving field is customized using the Lyapunov control theory. Lyapunov control has been proven to be a sufficiently simple control technology [38–44]. By designing an external controller in open- and closed-loops, one can avoid impossible or difficult measurements and feedback. Thus, it has been applied comprehensively in various tasks such as quantum state preparation [45–49], quantum gate implementation [50–52], quantum decoherence suppression [53], strong mechanical squeezing [54], and machine learning [55]. Using this powerful control technology, we show that arbitrary Fock states can be generated from their adjacent Fock states, while the generation of other nonclassical states is accomplished with a specific unitary transformation. One feature of the scheme is that the external nonlinear driving system is not necessary. Thus, the scheme avoids the decaying and decoherence effects of the external two-level driving system and sidesteps the infidelity caused by the higher-order terms of qubit-cavity coupling [35].

The rest of this paper is organized as follows: In Sec. II, we present the system model and review the general Lyapunov control theory. In Sec. III, we present a few examples by generating several typical nonclassical states. In Sec. IV, we investigate the robustness of the scheme. Conclusions are presented in Sec. V.

II. SYSTEM MODEL AND LYAPUNOV CONTROL THEORY

A. A driven anharmonic oscillator system

We consider an anharmonic oscillator which is driven by an external field with frequency ω . The Hamiltonian of the system is described by [56,57]

$$\hat{H} = \hbar\omega_0\hat{a}^\dagger\hat{a} + \hbar\chi(\hat{a}^\dagger\hat{a})^2 + \hbar f(t)[\Omega e^{-i\omega t}\hat{a}^\dagger + \text{H.c.}], \quad (1)$$

where \hat{a} (\hat{a}^\dagger) is the boson annihilation (creation) operator, ω_0 is the oscillatory frequency, χ is the strength of the anharmonicity, i.e., the strength of the photon-photon interaction proportional to the real part of the third-order nonlinear susceptibility $\text{Re}[\chi^{(3)}]$, and $\Omega f(t)$ is the time-dependent coupling strength, which is proportional to the amplitude of the external field. Note that the nonlinearity breaks the degeneracy of the oscillatory energy-level spacings in the absence of the drive. Here, we assume that the oscillator is driven by a single-photon process as described by the last term in Eq. (1) without considering the multi-photon driving process [58] and the higher order nonlinearities [59].

The Hamiltonian in Eq. (1) can be implemented in several physical systems. For instance, it can be used to describe the nanomechanical oscillator with \hat{a} and \hat{a}^\dagger related to the position

and momentum operators of a mode quantum motion [36],

$$\hat{x} = \sqrt{\frac{\hbar}{2m\nu}}(\hat{a} + \hat{a}^\dagger), \quad \hat{p} = -i\sqrt{2\hbar m\nu}(\hat{a} - \hat{a}^\dagger), \quad (2)$$

where m is the effective mass of the nanomechanical resonator, ν is the linear resonator frequency, and χ is proportional to the duffing nonlinearity. In addition, an optical cavity involving third-order nonlinearity under coherent driving is described by Eq. (1). The anharmonicity of the mode dynamics arises from its self-phase modulation caused by photon-photon interaction in the nonlinear medium [60]. The operators \hat{a} and \hat{a}^\dagger are the annihilation and creation operators for the single-mode of the cavity at frequency ω_0 , and Ω is the Rabi frequency corresponding to a classical coherent driving field. Quantum behaviours can be observed when cooling down the temperatures for which thermal energy is comparable to the energy of the oscillator quanta [61–63]. It also describes the variants of nano-oscillators based on a double-clamped platinum beam [64,65] and a single-light mode propagated in Kerr media [66,67].

Formally, the Hamiltonian in Eq. (1) can be written as

$$\hat{H} = \hat{H}_0 + \hat{H}_c(t), \quad (3)$$

where $\hat{H}_0 = \hbar\omega_0\hat{a}^\dagger\hat{a} + \hbar\chi(\hat{a}^\dagger\hat{a})^2$ describes the static Hamiltonian, and $\hat{H}_c(t) = \hbar f(t)(\Omega e^{-i\omega t}\hat{a}^\dagger + \text{H.c.})$ illustrates the control part of the system. The driven anharmonic oscillator system has been widely studied in the context of stochastic resonance [68] and quantum dissipative chaos [69,70]. In the absence of classical driving, i.e., $f(t) = 0$, the quantized vibration states of the nonlinear oscillator are the Fock states $|n\rangle$. Namely, the static Hamiltonian H_0 satisfies the eigenequation $\hat{H}_0|n\rangle = E_n|n\rangle$, where the eigenenergy $E_n = \hbar\omega_0 n + \hbar\chi n^2$ with $n = 0, 1, 2, \dots$. The levels $|n\rangle$ form an anharmonic ladder with the anharmonicity given by $E_{21} - E_{10} = 2\hbar\chi$, where $E_{mm} = E_m - E_n$. Regardless of the anharmonicity, the energetic spectrum also shifts in the case of monochromatic excitation [36].

B. Field design based on Lyapunov control

Lyapunov control is a powerful technique for quantum control tasks, which consists of two steps. The first step is the numerical calculation of the time-dependent control fields by simply simulating the system dynamics in the feedback form. In the second step, the generated control fields are used in an open-loop. We introduce the general formula of quantum Lyapunov control for the closed quantum system described by the Liouville equation (we assume $\hbar = 1$ hereafter),

$$\frac{d\hat{\rho}(t)}{dt} = -i[\hat{\mathcal{H}}_0 + \sum_{k=1}^K f_k(t)\hat{\mathcal{H}}_k, \hat{\rho}(t)], \quad (4)$$

where $\hat{\mathcal{H}}_0$ is the drift Hamiltonian of the system, $\hat{\mathcal{H}}_k$ are the control Hamiltonians, and $f_k(t)$ are the corresponding control fields which are realizable, scalar, real-valued time-dependent functions. The basic principle of Lyapunov control is to find proper control fields $f_k(t)$ to steer the quantum system into a target state $\hat{\rho}_T$, one of the eigenstates of $\hat{\mathcal{H}}_0$. To find such control fields, we should first select a real function called Lyapunov function $V(t)$. Notice that the choice of Lyapunov

function is not unique. Here we consider the following form of Lyapunov function based on the trace distance (state-based Lyapunov control in the density matrix form) [53],

$$V(t) = 1 - \text{Tr}[\hat{\rho}(t)\hat{\rho}_T]. \quad (5)$$

Obviously, the Lyapunov function $V(t)$ is semidefinite [$V(t) \geq 0$] and takes the minimum value only when the system converges to the target state. The control fields are designed by means of the first-order time derivative of $V(t)$, which satisfies $\dot{V}(t) \leq 0$. It is not hard to calculate that

$$\dot{V}(t) = - \sum_{k=1}^K f_k(t) \text{Tr}(\rho_T \{-i[\hat{\mathcal{H}}_k, \hat{\rho}(t)]\}). \quad (6)$$

Then the control fields can be chosen as the following form

$$f_k(t) = A_k \text{Tr}(\rho_T \{-i[\hat{\mathcal{H}}_k, \hat{\rho}(t)]\}), \quad (7)$$

where the positive parameters A_k are adopted to adjust the amplitude of the control fields. An increase in the value of A_k leads to a reduction of the duration of the control. With the designed control fields in Eq. (7), the Lyapunov function $V(t)$ keeps nonincreasing in the controlled dynamics. In other words, any initial state $\rho(0)$ [except for the one that satisfies $\dot{V}(0) = 0$] will asymptotically converge to the target state $\hat{\rho}_T$.

The convergence behavior can be analyzed by LaSalle's invariant principle [71,72]. As a prerequisite of Lyapunov control, the drift Hamiltonian $\hat{\mathcal{H}}_0$ and the control Hamiltonian $\hat{\mathcal{H}}_k$ should satisfy certain conditions. The drift Hamiltonian $\hat{\mathcal{H}}_0$ should be strongly regular, i.e., the transition frequencies between the target state and other eigenstates are distinguishable [44]. At the same time, the control Hamiltonian $\hat{\mathcal{H}}_k$ should contain a direct coupling between the target state and other eigenstates of $\hat{\mathcal{H}}_0$. When these conditions are satisfied, the system will necessarily converge to an invariant set $E = \{\hat{\rho}_T : \dot{V}(t) = 0\}$ with the designed control fields.

C. Generation of nonclassical states in a nonlinear oscillator

To generate the target Fock state $|n\rangle$ in the considered anharmonic oscillator system, we chose the drift Hamiltonian $\hat{\mathcal{H}}_0 = \hat{H}_0$ in Eq. (3). The control part of the system is $\hat{H}_c(t) = f(t)(\Omega e^{-i\omega t} \hat{a}^\dagger + \text{H.c.})$, where the strength of the external driving field $f(t)$ is designed by Lyapunov control. It is seen from the Hamiltonian \hat{H}_0 that the oscillatory levels are well resolved in the case of nonvanishing anharmonicity, i.e., $E_{mn} \neq E_{lj}$ ($m \neq n \neq l \neq j$). Thus, the transition frequencies between the target Fock state and other eigenstates (Fock states) are distinguishable. For the control Hamiltonian of the considered anharmonic oscillator system, however, the condition that there should exist direct coupling between the target Fock state and other eigenstates of \hat{H}_0 is not strictly satisfied. We can see from \hat{H}_c that Fock state $|n\rangle$ is only directly coupled to the adjacent Fock states $|n \pm 1\rangle$. Therefore, we cannot generate the target Fock state $|n\rangle$ with an arbitrary initial state by using state-based Lyapunov control. In other words, the generation of the target Fock state $|n\rangle$ relies on the initial state of the system due to the limitation of the control Hamiltonian of the system. However, the high-lying arbitrary Fock state $|n\rangle$ is realizable step-by-step, i.e., the target Fock state $|n\rangle$ can be generated in certain conditions by choosing the initial state

as $|n-1\rangle$ ($n = 1, 2, \dots$). Alternatively, due to the flexibility in choosing the Lyapunov function, the dependence of the generation of the target Fock state on the initial state can be avoided by using an average-value-based Lyapunov control [73,74].

On the other hand, the Lyapunov control can also be used to generate the superpositions of Fock states, $|\psi_T\rangle = \sum_n c_n |n\rangle$, where the complex coefficients c_n satisfy $\sum_n |c_n|^2 = 1$. Note that the target superposition state is no longer the eigenstate of \hat{H}_0 , which leads to the first-order time derivative of $V(t)$ as

$$\dot{V}(t) = -f(t) \text{Tr}(\hat{\rho}_T \{-i[\hat{H}_c, \hat{\rho}(t)]\}) - \text{Tr}\{-i\hat{\rho}_T[\hat{H}_0, \hat{\rho}(t)]\}, \quad (8)$$

where $\hat{\rho}_T = |\psi_T\rangle\langle\psi_T|$. Due to the existence of the second term on the right-hand side, it is difficult to guarantee $\dot{V}(t) \leq 0$ and then design the control fields. To determine the sign of $\dot{V}(t)$ and obtain control fields that are suitable for the generation of arbitrary superpositions of Fock states, we resort to a specific unitary transformation for the system, with the unitary operator defined as $\hat{U}(t) = \text{diag}\{e^{-iE_0 t}, e^{-iE_1 t}, \dots, e^{-iE_n t}\}$ [75]. The evolution of the system with respect to the rotating frame is (we refer to such a frame as the ‘‘rotating frame’’)

$$\frac{d\hat{\rho}'(t)}{dt} = -i[\hat{H}'_0 + f(t)\hat{H}'_c - \hat{\Lambda}, \hat{\rho}'(t)], \quad (9)$$

where $\hat{H}'_0 = \hat{U}^\dagger \hat{H}_0 \hat{U}$, $\hat{H}'_c = \hat{U}^\dagger \hat{H}_c \hat{U}$, $\hat{\rho}'(t) = \hat{U}^\dagger \hat{\rho}(t) \hat{U}$, and $\hat{\Lambda} = \text{diag}\{E_0, E_1, \dots, E_n\}$. Then the first-order time derivative of $V(t)$ is

$$\dot{V}(t) = -f(t) \text{Tr}(\hat{\rho}'_T \{-i[\hat{H}'_c, \hat{\rho}'(t)]\}), \quad (10)$$

where $\hat{\rho}'_T = \hat{U}^\dagger \hat{\rho}_T \hat{U}$. Now it is easy to choose the control field that satisfies the condition of $\dot{V}(t) \leq 0$, such as

$$f(t) = A_c \text{Tr}(\hat{\rho}'_T \{-i[\hat{H}'_c, \hat{\rho}'(t)]\}). \quad (11)$$

Based on the Lyapunov control, in the rotating frame, we can deterministically drive the initial state $\hat{\rho}'(0)$ to the state $\hat{\rho}'_T$ with the designed control field shown above. It is clear from Eq. (10) that when the system approaches $\hat{\rho}'_T$, the first-order time derivative of $\dot{V}(t) \rightarrow 0$. In that case, the control field given by Eq. (11) vanishes. Notice that since the target state $\hat{\rho}_T$ is no longer the eigenstate of \hat{H}_0 , the system is unstable if we move back to the original frame; even the control field vanishes. In other words, $\frac{d\hat{\rho}(t)}{dt} = -i[\hat{H}_0, \hat{\rho}(t)] \neq 0$ even if $\hat{\rho}(t) \rightarrow \hat{\rho}_T$ due to $[\hat{H}_0, \hat{\rho}_T] \neq 0$. However, the target superpositions of Fock states $|\psi_T\rangle$ in the original frame can be achieved at a specific time. Concretely, in the rotating frame, we can set the target state as $|\psi'_T\rangle = \sum_n c_n e^{-iH_0 t_f} |n\rangle = \sum_n c_n e^{-iE_n t_f} |n\rangle$. Such a state can be obtained in the rotating frame with the designed control field given by Eq. (11). Then the target superpositions of Fock state $|\psi_T\rangle$ is achieved at time t_f when we move back to the original frame, i.e.,

$$|\psi(t)\rangle = \hat{U}^\dagger(t) |\psi'(t)\rangle \xrightarrow{|\psi'(t)\rangle \rightarrow |\psi'_T\rangle} \hat{U}^\dagger(t) \sum_n c_n e^{-iE_n t_f} |n\rangle \xrightarrow{t=t_f} \sum_n c_n |n\rangle. \quad (12)$$

It is worth mentioning that the time t_f is adjustable, but it should be long enough for completing the driving process:

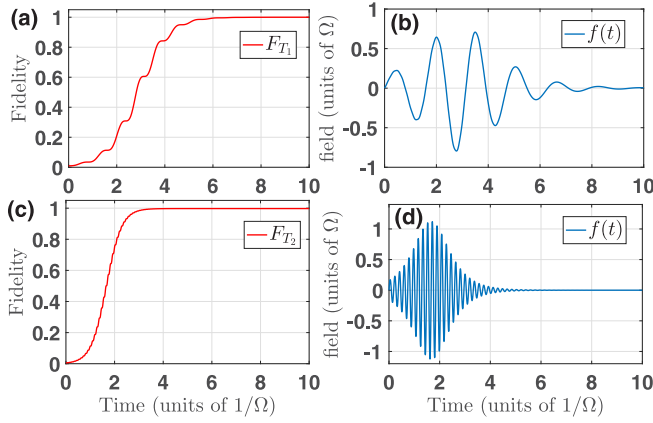


FIG. 1. Fidelity (a) and the corresponding control field (b) as a function of time for the generation of target Fock state $|1\rangle$. Fidelity (c) and the corresponding control field (d) as a function of time for the generation of target Fock state $|2\rangle$. The parameters are as follows: $\alpha = 0.1$, $\omega_0 = 11\Omega$, $\omega = -2\omega_0$, $\chi = 15\Omega$, and $A_c = 0.8/\Omega$.

$|\psi'(0)\rangle \rightarrow |\psi'_T\rangle$. Clearly, when we choose particular complex coefficients c_n , we can obtain different desired nonclassical states, such as Schrödinger-cat states, displaced Fock states, squeezed coherent states, etc., since these nonclassical states are the superpositions that have a definite phase relationship between Fock states.

III. NUMERICAL EXAMPLES

A. Fock states

In the previous section, we showed the feasibility of the scheme with respect to generating nonclassical states such as Fock states and arbitrary superpositions of Fock states. In the following, we demonstrate the generation of these states in the anharmonic oscillator system with concrete examples. To begin with, we generate Fock states by taking the two states $|1\rangle$ and $|2\rangle$ as examples. The simulation results of the fidelity $F_{T_n} = \sqrt{\sqrt{\hat{\rho}_{T_n}}\hat{\rho}(t)\sqrt{\hat{\rho}_{T_n}}}$ are presented in Fig. 1, where the target Fock state $\hat{\rho}_{T_n} = |n\rangle\langle n|$ ($n = 1, 2$), and $\rho(t)$ is numerically solved from Eq. (4). Figure 1(a) shows the production of Fock state $|1\rangle$ by considering the initial system in a coherent state $|\alpha\rangle = \hat{D}(\alpha)|0\rangle$, where $\hat{D}(\alpha) = e^{\alpha\hat{a}^\dagger - \alpha^*\hat{a}}$ is the Glauber displacement operator with α being a small complex number. The corresponding control field for generating Fock state $|1\rangle$ is obtained from Eq. (7) and shown in Fig. 1(b). From the simulation, one observes that the high fidelity of the target Fock state $|1\rangle$ is achieved after a time evolution of about $6/\Omega$. The control field approaches zero when the target state is obtained [see from Fig. 1(b)]. In addition, the fidelity F_{T_2} of target Fock state $|2\rangle$ is shown in Fig. 1(c) with the initial system in a displaced Fock state $|\alpha_d\rangle = \hat{D}(\alpha)|1\rangle$, and the corresponding control field is plotted in Fig. 1(d). We can see that the fidelity of target Fock state $|2\rangle$ assumes a consistent evolution with a high value after evolution time $4/\Omega$ [see Fig. 1(c)] due to the nearly zero control field [see Fig. 1(d)]. Clearly, there is no need to precisely control the evolution time for generating Fock states.

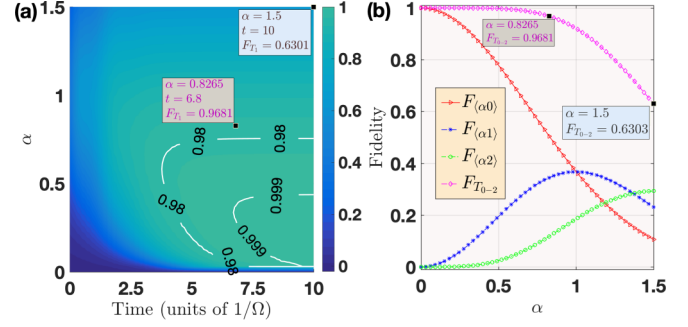


FIG. 2. (a) Fidelity F_{T_1} as a function of time and α for the generation of target Fock state $|1\rangle$. (b) Fidelity $F_{(\alpha j)}$ and $F_{T_{0-2}}$ as a function of α . The parameters are as follows: $\omega_0 = 11\Omega$, $\omega = -2\omega_0$, $\chi = 15\Omega$ and $A_c = 0.8/\Omega$.

Note that two aspects should be emphasized in the generation of Fock states. On the one hand, since the density matrix form of the state-based Lyapunov control is independent of the phase factor of the system state, i.e., $V(|\psi(t)\rangle) = V(e^{i\phi}|\psi(t)\rangle)$ ($\phi \in \mathbb{R}$), we cannot achieve state steering if the initial state of the system is an eigenstate of \hat{H}_0 and satisfies $\langle\psi(0)|\psi_T\rangle = 0$ [44]. Therefore, we are unable to generate the target Fock state from another Fock states. For instance, the generation of Fock state $|n\rangle$ from $|m\rangle$ ($n \neq m$) is unavailable. This is a result of the fact that both Fock states are the eigenstate of the drift Hamiltonian \hat{H}_0 and they are orthogonal to each other, resulting in the null control fields in Eq. (7) all the time. Therefore, we prepare the system initially in a coherent (displaced Fock) state with a small amplitude $\alpha = 0.1$ to avoid such a situation in the production of Fock state $|1\rangle$ ($|2\rangle$). In this case, one can note that the initial state $|\alpha\rangle$ ($|\alpha_d\rangle$) is not strictly orthogonal to target Fock state $|1\rangle$ ($|2\rangle$), with the overlap $|\langle\alpha|1\rangle|^2 \simeq 10^{-3}$ ($|\langle\alpha_d|2\rangle|^2 \simeq 10^{-2}$). To directly generate Fock state $|n\rangle$ from $|m\rangle$, an alternative technique is to add a small disturbance to the initial control field to trigger the evolution of the system [50]. This is exactly the technique that is used for the transmission of photons between two cavities, where the coupling coefficient has nonzero initial values [76].

On the other hand, we are unable to generate the target Fock state $|n\rangle$ from other Fock states except for $|n \pm 1\rangle$ even at the case that the orthogonal problem is solved due to the fact that there are no direct couplings between the target Fock state and other Fock states except $|n \pm 1\rangle$ in the control Hamiltonian \hat{H}_c . We verify this point in Fig. 2 by simulating the fidelity F_{T_1} as a function of amplitude α and time. According to Fig. 2(a), we obtain the following results: (i) We cannot generate the target Fock state $|1\rangle$ if the system is initially in vacuum state $|0\rangle$ [see from Fig. 2(a) where $F_{T_1} = 0$ in the case of $\alpha = 0$]. (ii) The high fidelity of target Fock state $|1\rangle$ is obtained by increasing the value of α in certain ranges. For instance, F_{T_1} reaches 0.999 if $0 < \alpha < 0.47$ after enough operation time, which can be seen from the white line in Fig. 2(a). (iii) When further increasing the value of α , the target fidelity gradually decreases, meaning that the target state is unreachable if the value of α is too large. (iv) The time for generating the high-fidelity target state decreases when increasing the value of α , such as $F_{T_1} = 0.98$, shown by the white line.

Result (i) is due to the aforementioned orthogonal problem, and the reasons for the remaining results can be illuminated by simulating the fidelity $F_{(\alpha j)} = |\langle \alpha | j \rangle|^2$ and $F_{T_{0-2}} = \sum_j F_{(\alpha j)}$ ($j = 0, 1, 2$) as a function of amplitude α , as shown in Fig. 2(b). Upon inspection of the dash-cyan line in Fig. 2(b), one can note that the fidelity $F_{T_{0-2}}$ is closest to the unit if the value of α is less than 0.5, and it decreases when further increasing the value of α . This is why we obtain the results (ii) and (iii). Then, in turn, it illustrates the point that we are unable to produce the target Fock state $|n\rangle$ from other Fock states except $|n \pm 1\rangle$. To be specific, one can note that the fidelity F_{T_1} in Fig. 2(a) matches well the fidelity $F_{T_{0-2}}$ in Fig. 2(b) after enough operational time with the same value of α . For instance, as shown by the black points in Fig. 2(a), the fidelity $F_{T_1} = 0.9681$ ($F_{T_1} = 0.6301$) when $\alpha = 0.8265$ ($\alpha = 1.5$) at the time $6.8/\Omega$ ($10/\Omega$). In such a case, the fidelity almost coincides with the fidelity $F_{T_{0-2}}$ in Fig. 2(b), if we choose the same value of α [see from the black points in Fig. 2(b)]. This means that only the components of states $|0\rangle$ and $|2\rangle$ can be transferred to target state $|1\rangle$, while the component of state $|1\rangle$ in the initial coherent state remains unchanged. This is exactly the reason why we obtain the result (iv). We can see from the blue-dash line in Fig. 2(b) that the fidelity $F_{(\alpha 1)}$ increases when increasing the value of α in the range $[0, 1]$. Thus, in generating the high-fidelity target Fock state $|1\rangle$, there are fewer components (states $|0\rangle$ and $|2\rangle$) to be transferred when increasing the value of α , resulting in less time for generating the high-fidelity target state as shown in Fig. 2(a).

Here, we characterize the nonclassical property of the generated states by the Wigner function, which describes the quasi-probability distribution in the complex phase space for quantum states [77]. The Wigner function associated with the density operator $\hat{\rho}(t)$ is described by

$$W(t, r, \theta) = \sum_{m,n} \rho_{mn}(t) W_{nm}(r, \theta), \quad (13)$$

where $\rho_{mn}(t) = \langle m | \hat{\rho}(t) | n \rangle$ are the matrix elements of the density operator in the Fock state representation, (r, θ) are the polar coordinates in the phase space plane $X = r \cos \theta$, $Y = r \sin \theta$, whereby the coefficients W_{nm} are the Fourier transform of the matrix elements of the Wigner characteristic function [36]. This quantity is always nonnegative if the state $\hat{\rho}(t)$ is a classical mixture, and the observation of negative values in regions of phase space is a signature of quantum interference.

We display the Wigner function of the pure Fock states $|1\rangle$ and $|2\rangle$ in Figs. 3(a) and 3(c), respectively. For contrast, the Wigner functions $W(t_F, r, \theta)$ of the corresponding generated Fock states $|1\rangle$ and $|2\rangle$ at final time t_F are presented in Figs. 3(b) and 3(d), respectively. Clearly, upon observation of Figs. 3(a) and 3(b) [as well as Figs. 3(c) and 3(d)] one can draw the conclusion that the shape of the Wigner functions for the pure Fock state $|1\rangle$ ($|2\rangle$) and the generated state match well. This demonstrates that these nonclassical states are successfully obtained by the Lyapunov control.

B. Arbitrary superpositions of Fock states

Next, we show the performance of the scheme for the generation of arbitrary superpositions of Fock states in the an-

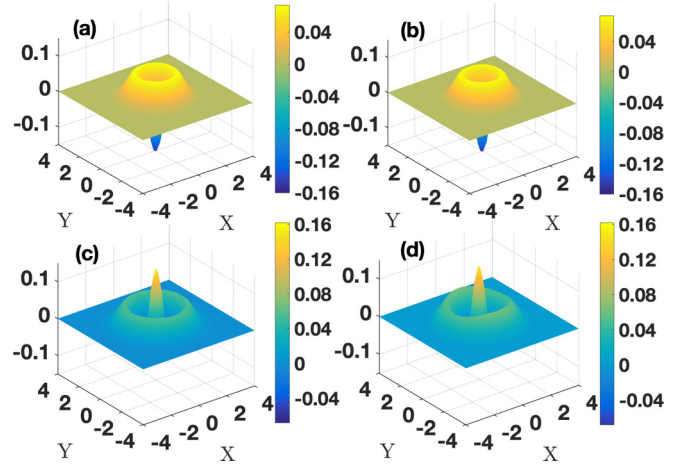


FIG. 3. (a) The Wigner function for the pure Fock state $|1\rangle$. (b) The calculated Wigner function $W(t_F, r, \theta)$ in generating target Fock state $|1\rangle$ at evolution time t_F . (c) The Wigner function for the pure Fock state $|2\rangle$. (d) The calculated Wigner function $W(t_F, r, \theta)$ in generating target Fock state $|2\rangle$ at evolution time t_F . The parameters are as follows: $\alpha = 0.1$, $\omega_0 = 11\Omega$, $\omega = -2\omega_0$, $\chi = 15\Omega$, $A_c = 0.8/\Omega$, and $t_F = 10/\Omega$.

harmonic oscillator system. We take the target superposition states $|T_1^s\rangle$ and $|T_2^s\rangle$ as examples. The simulation is performed by numerically solving Eq. (9) with the field given by Eq. (11). Note that during the generation of target state $|T_1^s\rangle$, in the rotating frame, we choose the state $\hat{\rho}'_T = |\psi'_T\rangle\langle\psi'_T|$ to design the control field, with $|\psi'_T\rangle = e^{-iE_n t_f} |T_1^s\rangle$. The simulation results of the fidelity $F_{T_1^s}^R = \sqrt{\langle \hat{\rho}'_T | \hat{\rho}'(t) | \hat{\rho}'_T \rangle}$ in the rotating frame are presented in Fig. 4(a), with the system initially in a coherent state $|\alpha_0^s\rangle$. The corresponding control field is shown in Fig. 4(b). From the simulation results, we can observe that

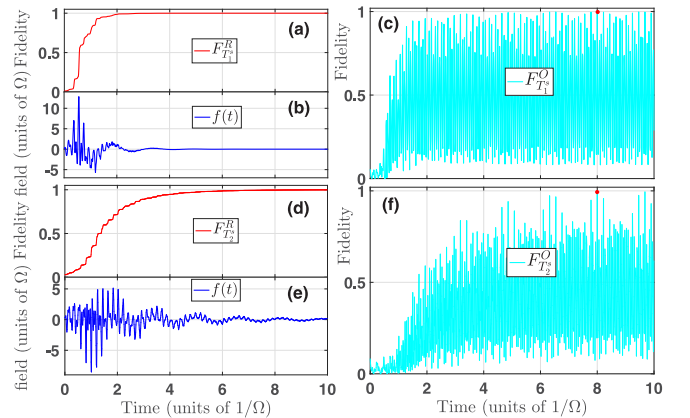


FIG. 4. For the generation of target superposition state $|T_1^s\rangle = (|1\rangle + 2|2\rangle + 3|3\rangle)/\sqrt{14}$, (a) fidelity $F_{T_1^s}^R$ and (b) the corresponding control field as a function of time. (c) Fidelity $F_{T_1^s}^O$ as a function of time. For the generation of target superposition state $|T_2^s\rangle = (|0\rangle + |1\rangle + 2|2\rangle + 3|3\rangle + 5|4\rangle)/\sqrt{40}$, (d) fidelity $F_{T_2^s}^R$, and (e) the corresponding control field as a function of time. (f) Fidelity $F_{T_2^s}^O$ as a function of time. The parameters are as follows: $\alpha_0^s = 2.5$, $\omega_0 = 11\Omega$, $\omega = -2\omega_0$, $\chi = 15\Omega$, $t_{f_1} = t_{f_2} = 8/\Omega$, and $A_c = 15/\Omega$.

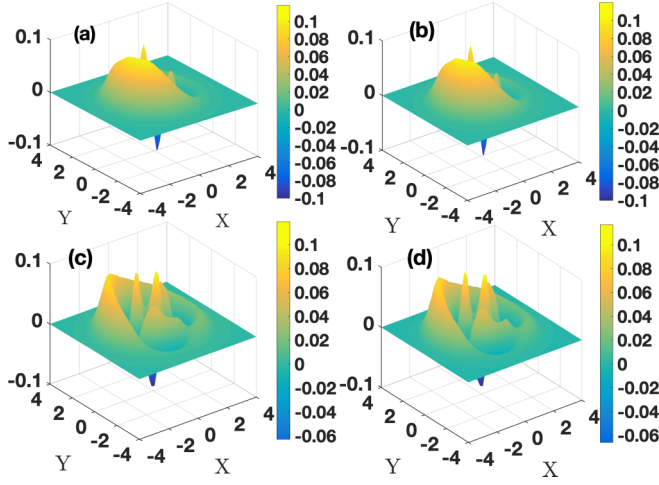


FIG. 5. (a) The Wigner function for the pure superposition state $|T_1^s\rangle$. (b) The calculated Wigner function $W(t_F, r, \theta)$ in generating target state $|T_1^s\rangle$ at evolution time t_F . (c) The Wigner function for the pure the pure superposition state $|T_2^s\rangle$. (d) The calculated Wigner function $W(t_F, r, \theta)$ in generating target state $|T_2^s\rangle$ at evolution time t_F . The parameters are as follows: $\alpha_0^s = 2.5$, $\omega_0 = 11\Omega$, $\omega = -2\omega_0$, $\chi = 15\Omega$, $t_{f_1} = t_{f_2} = 8/\Omega$, and $A_c = 15/\Omega$.

the fidelity $F_{T_1^s}^R$ rapidly reaches 0.99 after time $2/\Omega$. The control field is approximate to zero when the fidelity reaches that high value. Notice that due to $[\hat{H}_0, |T_1^s\rangle\langle T_1^s|] \neq 0$, the system in the original frame would evolve under the Hamiltonian \hat{H}_0 so that even the control field vanishes. However, the target state $|T_1^s\rangle$ can be obtained at a specific time. To illustrate this point, the evolution of fidelity $F_{T_1^s}^O = \sqrt{\langle \hat{\rho}_T | \hat{\rho}(t) | \hat{\rho}_T \rangle}$ in the original frame is depicted in Fig. 4(c), where $\hat{\rho}_T = |T_1^s\rangle\langle T_1^s|$. It is clear that the target state $|T_1^s\rangle$ is achieved at time $t_{f_1} = 8/\Omega$. Similarly, for the generation of $|T_2^s\rangle$, in the rotating frame, the state $|\psi'_T\rangle = e^{-iE_n t_{f_2}} |T_2^s\rangle$ is chosen to design the control field.

The simulation result of the fidelity $F_{T_2^s}^R = \sqrt{\langle \hat{\rho}'_T | \hat{\rho}'(t) | \hat{\rho}'_T \rangle}$ is presented in Fig. 4(d), with the corresponding control field shown in Fig. 4(e). We can observe that the fidelity $F_{T_2^s}^R$ gradually increases to 0.996 after time $8/\Omega$, indicating that the state $\hat{\rho}'_T$ is obtained in the rotating frame. When we move back to the original frame, the target state $|T_2^s\rangle$ is also achieved at $t_{f_2} = 8/\Omega$, as seen from the red point in Fig. 4(f) in which the fidelity $F_{T_2^s}^O = \sqrt{\langle \hat{\rho}_T | \hat{\rho}(t) | \hat{\rho}_T \rangle}$ is plotted, where $\hat{\rho}_T = |T_2^s\rangle\langle T_2^s|$.

In addition, to show the nonclassical property of the target superposition states $|T_1^s\rangle$ and $|T_2^s\rangle$, we plot the Wigner function of pure $|T_1^s\rangle$ in Fig. 5(a) and $|T_2^s\rangle$ in Fig. 5(c). The corresponding states generated by Lyapunov control are shown in Figs. 5(b) and 5(d), respectively. As apparent from Figs. 5(a) and 5(b), as well as from Figs. 5(c) and 5(d), the states generated by the Lyapunov control match well the pure target superposition states $|T_1^s\rangle$ and $|T_2^s\rangle$, respectively.

C. Coherent states

In the following, we investigate the performance of the scheme in generating nonclassical states that have a definite phase relationship between Fock states, and we discuss their

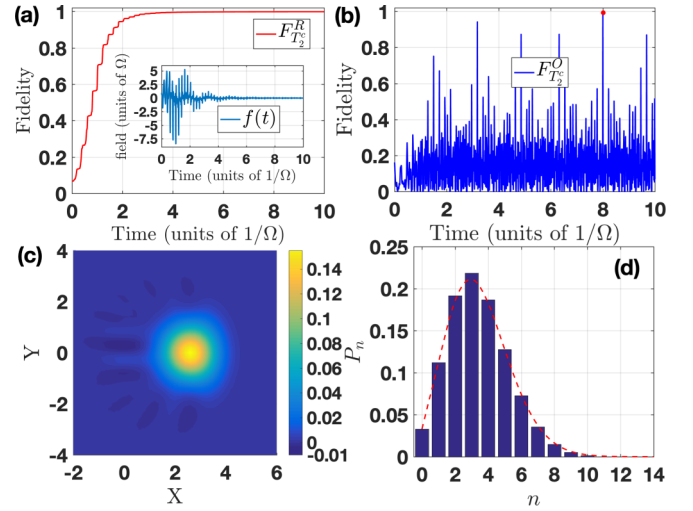


FIG. 6. Fidelity $F_{T_2^s}^R$ (a) and the corresponding control field (the inset) as a function of time for generating target coherent state $|\zeta_2\rangle$. (b) Fidelity $F_{T_2^s}^O$ as a function of time. (c) The calculated Wigner function of the generated coherent state $|\zeta_2\rangle$ at evolution time t_f . (d) The probabilities of the Fock state components in the generated coherent state $|\zeta_2\rangle$, fitted by a Poissonian distribution (the red-dash line) with $\bar{n} \simeq 3.4$. The parameters are as follows: $\zeta_1 = 0.5$, $\zeta_2 = 1.85$, $\omega_0 = 11\Omega$, $\omega = -2\omega_0$, $\chi = 15\Omega$, $A_c = 10/\Omega$, and $t_f = 8/\Omega$.

nonclassical properties. As an example, we first show that the scheme is feasible for generating the coherent state $|\zeta_2\rangle$ from another coherent state $|\zeta_1\rangle$. For the coherent states, it is well known that the distribution among Fock states is Poissonian, $P_n = \bar{n}^n \exp(-\bar{n})/n!$, where \bar{n} is the average quantum number [78].

In Fig. 6(a), in the rotating frame, we show the process of $|\zeta_1\rangle \rightarrow e^{-iE_n t_f} |\zeta_2\rangle$ by simulating the fidelity $F_{T_2^s}^R = \sqrt{\langle \hat{\rho}'_{T_2^s} | \hat{\rho}'(t) | \hat{\rho}'_{T_2^s} \rangle}$ as a function of time, where $\hat{\rho}'_{T_2^s} = |\psi'_T\rangle\langle \psi'_T|$ with $|\psi'_T\rangle = e^{-iE_n t_f} |\zeta_2\rangle$. The corresponding control field for this transferring process is given in the inset of Fig. 6(a). It is evident that the state $|\psi'_T\rangle$ is deterministically obtained after enough time. When moving back to the original frame, we display the evolution of fidelity $F_{T_2^s}^O = \sqrt{\langle \hat{\rho}_{T_2^s} | \hat{\rho}(t) | \hat{\rho}_{T_2^s} \rangle}$ in Fig. 6(b), where $\hat{\rho}_{T_2^s} = |\zeta_2\rangle\langle \zeta_2|$. As expected, the target coherent state $|\zeta_2\rangle$ is achieved at time $t_f = 8/\Omega$. In addition, we show the Wigner function of such a generated coherent state $|\zeta_2\rangle$ in Fig. 6(c), which displays small negative values in the phase space. Figure 6(d) shows the probabilities P_n of the Fock state components for the generated coherent state $|\zeta_2\rangle$. These amplitudes display the expected Poissonian dependence on n .

D. Squeezed coherent states

As another example, we next show the generation of squeezed coherent states, since these states can also be represented by the superposition of Fock states. The combined action of $\hat{D}(\alpha)$ followed by $\hat{S}(\xi)$ on the vacuum state $|0\rangle$ produces a class of squeezed coherent states [79],

$$|\xi, \alpha\rangle = \hat{S}(\xi)\hat{D}(\alpha)|0\rangle, \quad (14)$$

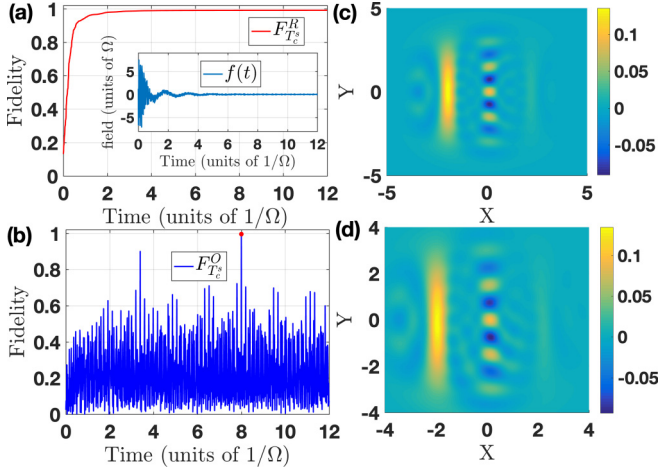


FIG. 7. Fidelity $F_{T_s^s}^R$ (a) and the corresponding control field (the inset) as a function of time for generating target squeezed coherent state $|\xi, \alpha\rangle$. (b) Fidelity $F_{T_s^s}^O$ as a function of time. (c) The Wigner function for the pure target squeezed coherent state $|\xi, \alpha\rangle$. (d) The calculated Wigner function of the generated squeezed coherent state via Lyapunov control at evolution time t_f . The initial state of system is in a coherent state $|\alpha\rangle$. The parameters are as follows: $\alpha = \sqrt{5}$, $r = 0.85$, $\phi = 0$, $\omega_0 = 11\Omega$, $\omega = -2\omega_0$, $\chi = 15\Omega$, $A_c = 10/\Omega$, and $t_f = 8/\Omega$.

where $\hat{S}(\xi) = \exp(-\frac{\xi}{2}\hat{a}^{\dagger 2} + \frac{\xi^*}{2}\hat{a}^2)$ is the squeezing operator with $\xi = r \exp(i\phi)$, r is the squeezing parameter and ϕ defines the direction of the quadrature phase squeezing. The result for the generation of squeezed coherent state $|\xi, \alpha\rangle$ is presented in Fig. 7. Figure 7(a) displays the evolution of fidelity $F_{T_s^s}^R = \sqrt{\langle \hat{\rho}'_{T_s^s} | \hat{\rho}'(t) | \hat{\rho}'_{T_s^s} \rangle}$ (in the rotating frame), and the inset shows the corresponding control field, where $\hat{\rho}'_{T_s^s} = |\psi'_T\rangle\langle\psi'_T|$ with $|\psi'_T\rangle = e^{-iE_{nT_s}t_f}|\xi, \alpha\rangle$. It can be observed that the fidelity $F_{T_s^s}^R$ rapidly approaches unity, indicating that the state $|\psi'_T\rangle$ is achieved. Our goal is the generation of target state $|\xi, \alpha\rangle$, and thus in Fig. 7(b) we depict the evolution of fidelity $F_{T_s^s}^O = \sqrt{\langle \hat{\rho}_{T_s^s} | \hat{\rho}(t) | \hat{\rho}_{T_s^s} \rangle}$ (in the original frame), where $\hat{\rho}_{T_s^s} = |\xi, \alpha\rangle\langle\xi, \alpha|$. As can be seen, the target state $|\xi, \alpha\rangle$ is achieved at time $t_f = 8/\Omega$ with $F_{T_s^s}^O \simeq 0.99$.

To show the nonclassical property of the target state $|\xi, \alpha\rangle$ and the generated state, we plot the Wigner functions of the pure target state $|\xi, \alpha\rangle$ and the generated state in Figs. 7(c) and 7(d), respectively. From the results, we can observe that the Wigner function of the generated state is very similar to the Wigner function of the pure target state $|\xi, \alpha\rangle$. We observe the negative values of the Wigner function in phase space, indicating the nonclassical feature of the squeezed coherent state.

E. Schrödinger-cat states

Whether dead or alive, Schrödinger's cat is clearly a macroscopic object, and the state of being alive is distinguishable from the state of being dead. Therefore, to realize a Schrödinger cat, we require a superposition of two macroscopically distinguishable quantum states. Coherent state $|\zeta\rangle$

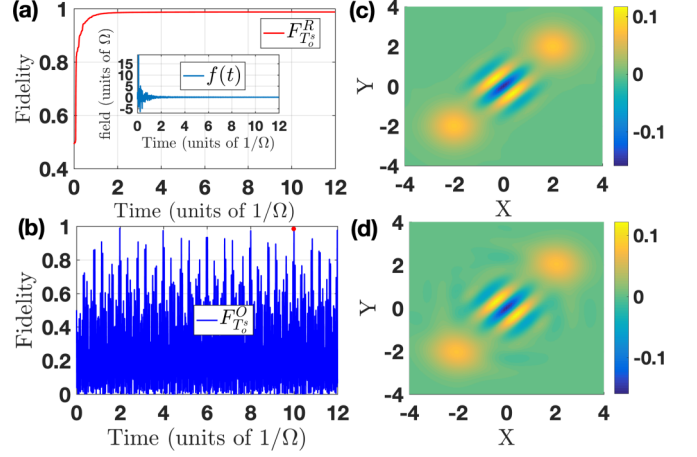


FIG. 8. Fidelity $F_{T_s^o}^R$ (a) and the corresponding control field (the inset) as a function of time for generating target even coherent state $|\Psi_o\rangle$. (b) Fidelity $F_{T_s^o}^O$ as a function of time. (c) The Wigner function for the pure target even coherent state $|\Psi_o\rangle$. (d) The calculated Wigner function of the generated even coherent state via Lyapunov control at evolution time t_f . The initial state of system is in a coherent state $|\zeta\rangle$. The parameters are as follows: $\zeta = \sqrt{5}$, $\omega_0 = 11\Omega$, $\omega = 2\omega_0$, $\chi = 15\Omega$, $A_c = \Omega$, and $t_f = 10/\Omega$.

seems to be a suitable candidate since its amplitude $|\zeta|^2$ can be arbitrarily large. As the distinguishable state, we chose another coherent state with the same amplitude but with a phase shift of π : $|\zeta\rangle$. For definiteness, we take the Schrödinger-cat state as the superposition [6],

$$|\Psi\rangle = \mathcal{N}[|\zeta\rangle + e^{i\phi}|\zeta\rangle], \quad (15)$$

where $\mathcal{N} = [2 + 2\cos(\phi)\exp(-2|\zeta|^2)]^{-1/2}$ is the normalization factor. The relative phase ϕ can be arbitrary. For $\phi = 0$, we obtain the even coherent states,

$$|\Psi_e\rangle = \mathcal{N}_e[|\zeta\rangle + |\zeta\rangle], \quad (16)$$

and for $\phi = \pi$, we obtain the odd coherent states,

$$|\Psi_o\rangle = \mathcal{N}_o[|\zeta\rangle - |\zeta\rangle], \quad (17)$$

where \mathcal{N}_e and \mathcal{N}_o are the normalization factors.

Here, we chose the generation of the odd coherent states as an example. Figure 8(a) shows the evolution of fidelity $F_{T_s^o}^R = \sqrt{\langle \hat{\rho}'_{T_s^o} | \hat{\rho}'(t) | \hat{\rho}'_{T_s^o} \rangle}$ in the rotating frame, where $\hat{\rho}'_{T_s^o} = |\psi'_T\rangle\langle\psi'_T|$ with $|\psi'_T\rangle = e^{-iE_{nT_s}t_f}|\Psi_o\rangle$. The inset of Fig. 8(a) shows the corresponding control field which is given by Eq. (11). We can observe that the state $|\psi'_T\rangle$ in the rotating frame is rapidly obtained, and the control field vanishes when achieving the goal. Figure 8(b) exhibits the evolution of fidelity $F_{T_s^o}^O = \sqrt{\langle \hat{\rho}_{T_s^o} | \hat{\rho}(t) | \hat{\rho}_{T_s^o} \rangle}$ in the original frame, where $\hat{\rho}_{T_s^o} = |\Psi_o\rangle\langle\Psi_o|$. The achieved high fidelity of $F_{T_s^o}^O$ at time $t_f = 10/\Omega$ indicates that the scheme is successful in generating Schrödinger-cat states. Figures 8(c) and 8(d) are the Wigner functions of the pure odd coherent state $|\Psi_o\rangle$ and the generated state at time t_f , respectively. The Wigner functions match very well and show ranges of negative values, indicating the nonclassical nature of these states.

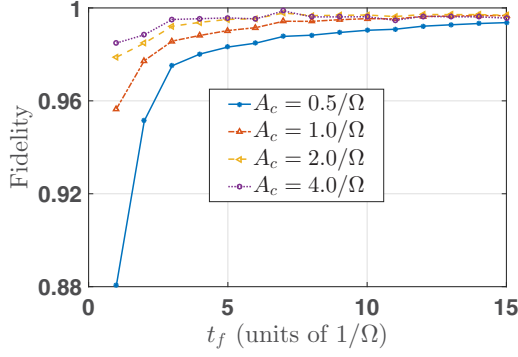


FIG. 9. Fidelity $F_{T_o}^O$ versus the time t_f under different value of A_c . The parameters are as follows: $\zeta = \sqrt{2}(1 + i)$, $\omega_0 = 11\Omega$, $\omega = 2\omega_0$, and $\chi = 15\Omega$.

IV. DISCUSSION

In the previous section, we showed that nonclassical states, including Fock states and superpositions of Fock states, can be obtained by using a Lyapunov control in the absence of any fluctuations and dissipation. In practice, the parameters in the drift Hamiltonian \hat{H}_0 may not faultlessly be obtained and the dissipation caused by decoherence mechanisms is ineluctable. These factors may cause a detrimental effect on the generation of nonclassical states. Therefore, we would like to check the performance of the scheme when these factors are taken into account.

We begin our discussion by showing the influence of different t_f on generating superpositions of Fock states. As we have pointed out, to achieve the target nonclassical state in the original frame, time t_f is adjustable, but it should be long enough for completing the generation of target state $|\psi'_T\rangle$ in the rotating frame. Here, we would like to check this point by taking the generation of Schrödinger-cat state $|\Psi_o\rangle$ as an example. In Fig. 9, we plot the fidelity $F_{T_o}^O$ versus time t_f with different values of A_c . It is clear from the plot that a high fidelity of target state is obtained when t_f is large enough. Moreover, to obtain the high fidelity of the target state in a short time, we can choose a large value of A_c . For instance, it requires $t_f > 5/\Omega$ for $F_{T_o}^O > 0.98$ when $A_c = 0.5/\Omega$, while we can ensure $F_{T_o}^O > 0.98$ as long as $t_f > 2/\Omega$ when $A_c = 2/\Omega$. This is a result of from the fact that the larger the value of A_c , the stronger the control field will be, resulting in a faster driving process of $\hat{\rho}'(0) \rightarrow \hat{\rho}'_T$ in the rotating frame.

To discuss the influence of anharmonicity χ on the generation of nonclassical states without loss of generality, we take the generation of superposition state $|\psi'_T\rangle = |T_1^s\rangle$ in the rotating frame as an example. Figure 10 shows the fidelity $F_{T_1^s}^R$ versus the strength of the anharmonicity χ and evolution time. Obviously, the superposition state $|\psi'_T\rangle$ is unreachable when the strength of anharmonicity χ vanishes, indicating that the existence of anharmonicity is important for the scheme. This is a consequence of the fact that the strong anharmonicity facilitates the resolution of the oscillatory levels and makes the drift Hamiltonian \hat{H}_0 strongly regular, i.e., the transition frequencies between the target state and other eigenstates are distinguishable, which is a prerequisite for Lyapunov control.

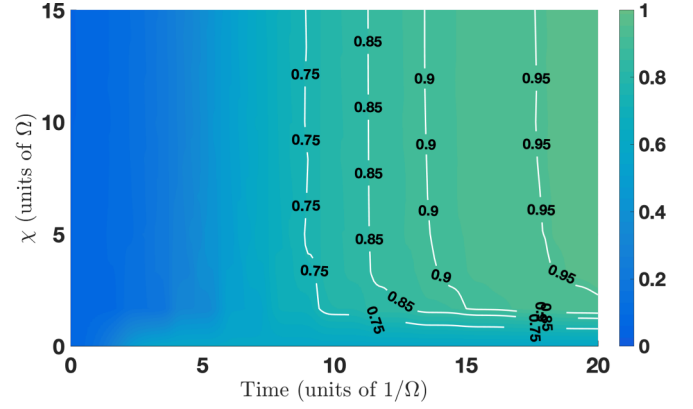


FIG. 10. Fidelity $F_{T_1^s}^R$ as a function of time and χ for generating target superposition state $|T_1^s\rangle$ in the rotating frame. The system is initially prepared in coherent state $|\alpha\rangle$. The parameters are as follows: $\alpha = 0.5$, $\omega_0 = 11\Omega$, $\omega = -2\omega_0$, and $A_c = 1/\Omega$.

We next discuss the influence of perturbations in the control field on generating the nonclassical states. We define the control field with perturbations as $f_\eta(t) = (1 + \eta)f(t)$, where η quantifies the strength of the perturbation. As an example, the effects of η on the generation of superposition state $|T_1^s\rangle$, squeezed coherent state $|\xi, \alpha\rangle$, and odd coherent state $|\Psi_o\rangle$, are shown in Fig. 11. As clearly seen from Fig. 11 the fidelities $F_{T_1^s}^R$, $F_{T_2^s}^R$, and $F_{T_c^s}^R$ are insensitive to the perturbations of the field, since these fidelities are only slightly changed even when $|\eta| = 5\%$, indicating that the present scheme is robust against perturbations in the control field. This stems from the principle of Lyapunov control, according to which the convergence process is more sensitive to the sign rather than the amplitude of the control field [74].

To illustrate the examples above, we assume that the initial state is the coherent state. For the nonlinear system, the initial finite dimensional coherent state can be generated by a weak external coherent field [80]. Specifically, a perfect initial coherent state is not required for the present scheme. To demonstrate this point, we assume that the initial state of the nonlinear system is $|\psi(0)\rangle = \frac{1}{\mathbf{N}} \sum_{n_0=0}^{N_f} c_{n_0} |n_0\rangle$ with \mathbf{N} being the normalization factor and N_f the truncated number. Using the generation of Fock state $|1\rangle$ and superpositions of

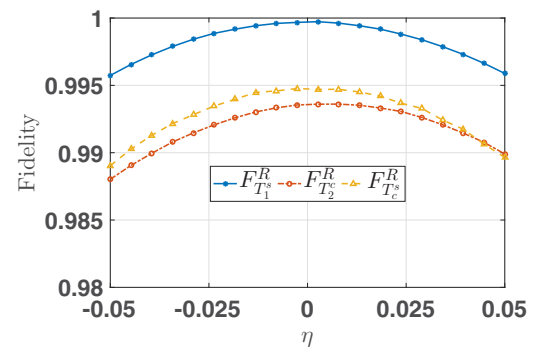


FIG. 11. The behaviour of fidelities $F_{T_2^s}^R$, $F_{T_c^s}^R$, and $F_{T_1^s}^R$ versus η . The parameters are the same with that given in Fig. 6 for $F_{T_2^s}^R$, Fig. 7 for $F_{T_c^s}^R$, and Fig. 8 for $F_{T_1^s}^R$.

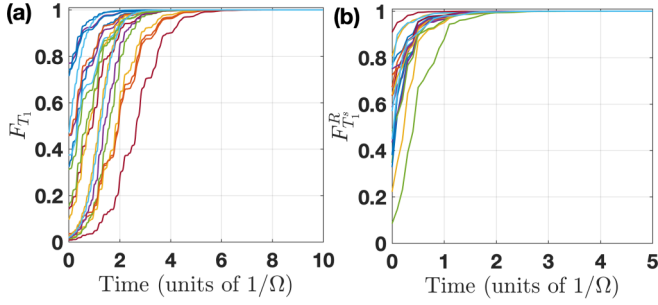


FIG. 12. Evolution of fidelity (a) F_{T_1} and (b) $F_{T_1^s}^R$ with 20 random initial states. The other parameters are the same with that given in Fig. 1 for F_{T_1} and Fig. 4 for $F_{T_1^s}^R$.

Fock states $|T_1^s\rangle$ as examples, we plot in Figs. 12(a) and 12(b) the evolution of fidelities F_{T_1} and $F_{T_1^s}^R$, respectively. In the simulations, 20 random initial states are considered with c_{n_0} being the random numbers uniformly created between 0 and 1. We set $N_t = 3$ for the generation of Fock state $|1\rangle$ and $N_t = 5$ for $|T_1^s\rangle$. The simulations show that all initial states converge to the target state, indicating that it is not necessary to prepare a perfect coherent state for the scheme.

In the above discussions, we did not take into account the interactions between the anharmonic oscillator system and the environment, which will inevitably affect the availability of the scheme. We now investigate the influence of dissipation and decoherence on the generation of nonclassical states. When these actual decoherence factors are taken into account, the accurate Lindblad master equation of the system can be expressed as [56,68]

$$\begin{aligned} \frac{d\hat{\rho}(t)}{dt} = & -i[\hat{\mathcal{H}}_0 + f(t)\hat{\mathcal{L}}_c, \hat{\rho}(t)] \\ & + \sum_{l=1,2} \left[\hat{L}_l \hat{\rho}(t) \hat{L}_l^\dagger - \frac{1}{2} \hat{L}_l^\dagger \hat{L}_l \hat{\rho}(t) - \frac{1}{2} \hat{\rho}(t) \hat{L}_l^\dagger \hat{L}_l \right], \end{aligned} \quad (18)$$

where $\hat{L}_1 = \sqrt{\gamma(\bar{n}+1)}\hat{a}$ and $\hat{L}_2 = \sqrt{\gamma\bar{n}}\hat{a}^\dagger$ are the Lindblad operators, γ is the dissipation rate, and \bar{n} represents the mean number of quanta of a heat bath.

As an example, we display the simulation results of the achieved nonclassical states, coherent state $|\zeta_2\rangle$, squeezed coherent state $|\xi, \alpha\rangle$, and odd coherent state $|\Psi_o\rangle$, by showing contour plots of the fidelities $F_{T_2^s}^R$, $F_{T_c^s}^R$, and $F_{T_o^s}^R$ as a function of γ and \bar{n} in Figs. 13(a), 13(b), and 13(c), respectively. We can see from the results that the fidelities $F_{T_2^s}^R$, $F_{T_c^s}^R$, and $F_{T_o^s}^R$ decrease with the increase in the dissipation rate γ when fixing \bar{n} , and the rate of decrease increases with \bar{n} . In addition, the dissipation and decoherence effect on the generation of the odd coherent state $|\Psi_o\rangle$ is greater than on the generation of coherent state $|\zeta_2\rangle$ and squeezed coherent state $|\xi, \alpha\rangle$. The results indicate that the influence of the dissipation and decoherence effect is different for the generation of different nonclassical states. However, we can see from Fig. 13(a) that the scheme is robust against the dissipation and decoherence effect for the generation of coherent state $|\zeta_2\rangle$, in which the fidelity is maintained at 93.5% even when $\{\bar{n}, \gamma\} = \{0.5, 0.01\Omega\}$. The simulation result shows that

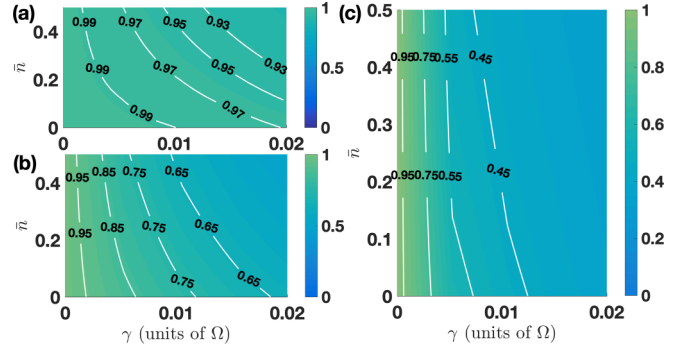


FIG. 13. The fidelity (a) $F_{T_2^s}^R$, (b) $F_{T_c^s}^R$, and (c) $F_{T_o^s}^R$ as a function of \bar{n} and γ . The parameters are the same with that given in Fig. 6 for $F_{T_2^s}^R$, Fig. 7 for $F_{T_c^s}^R$, and Fig. 8 for $F_{T_o^s}^R$.

although dissipation and decoherence have a detrimental effect on generating the nonclassical states, high-fidelity target nonclassical states are achievable in a certain range of dissipation rates.

We can now estimate the viability of the scheme in reference to the real parameters of a system of interest, such as a nonlinear oscillator composed of an optical cavity or superconducting cavity. We take the strength of anharmonicity χ to be $2\pi \times 0.016$ MHz. In Figs. 14(a) and 14(b), we show the fidelities F_{T_1} and $F_{T_2^s}^R$ as a function of time under different dissipation rate γ , respectively. We can observe that the fidelity of the generated Fock state $|1\rangle$ can be as high as 90% at time 100 μs when the coherence time of the cavity $T_1 = 0.5$ ms, which corresponds to $\gamma = 1/(0.5 \times 10^{-3})$ MHz (the red-solid-dot line). Although the fidelity F_{T_1} decreases with the time due to the dissipation, it can be improved by increasing the coherence time. When the coherence time T_1 of the cavity is increased to 10 ms, the nearly unit fidelity can be obtained (the magenta-dot-triangle line). Contrary to the behavior of F_{T_1} , which falls rapidly with time, $F_{T_2^s}^R$ can be maintained at a high value even when the coherence time T_1 is as short as 0.5 ms, which can be observed from Fig. 14(b).

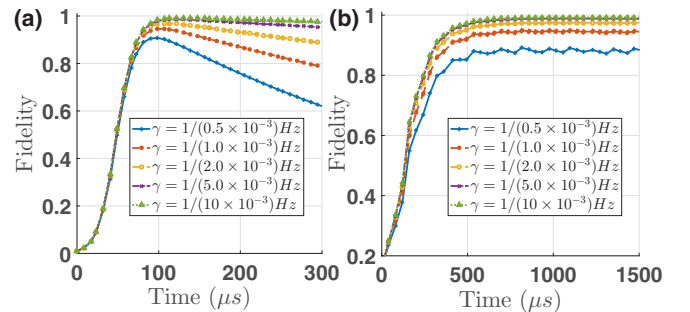


FIG. 14. (a) The fidelity F_{T_1} as a function of time under different dissipation rate γ . The initial state of the system is prepared in a coherent state $|\alpha\rangle$ with $\alpha = 0.1$. (b) The fidelity $F_{T_2^s}^R$ as a function of time under different dissipation rate γ . The initial state of the system is prepared in a coherent state $|\zeta_1\rangle$ and the final state is $|\zeta_2\rangle$ with $\zeta_1 = 0.5$ and $\zeta_2 = 1.85$. The other same parameters are: $\Omega = 2\pi \times 0.01$ MHz, $\omega_0 = \Omega$, $\omega = -2\Omega$, $A_c = 0.8/\Omega$, $\bar{n} = 0.0013$, and $\chi = 2\pi \times 0.016$ MHz.

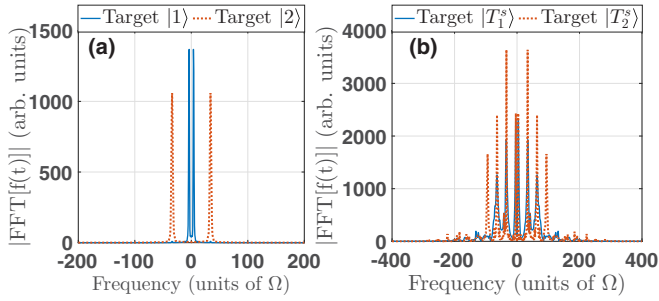


FIG. 15. (a) Discrete Fourier transform of the fields for generating the Fock states $|1\rangle$ and $|2\rangle$ with the same parameters of Fig. 1. (b) Discrete Fourier transform of the fields for generating the superpositions of Fock states $|T_1^s\rangle$ and $|T_2^s\rangle$ with the same parameters of Fig. 4.

This means that the scheme is more robust against dissipation for the generation of coherent states than for the generation of Fock states. Recent experiments on circuit quantum electrodynamics systems have shown that these real parameters can be obtained [81,85]. It has been shown by Xu *et al.* that the strength of anharmonicity $\chi \simeq 2\pi \times 0.016$ MHz and the coherence time $T_1 \simeq 0.5$ ms are observed in the superconducting cavity system [81].

In superconducting circuit experiments, the typical external control (GHz-level Digital-Analog-Convertor) dependent on the high-speed field programmable gate array (FPGA) based signal generator running at 1 GHz and with a bandwidth of 400 MHz is enough to generate the waveform for the specific control fields [81–84]. However, for other systems, such as optical cavities, it may be difficult to implement the scheme due to the complex waveform of the designed control fields. It can be seen from Figs. 1(b) and 1(d) that the waveforms of the fields for generating Fock states $|1\rangle$ and $|2\rangle$ are simple, but the fields for generating other nonclassical states are relatively complex, such as the fields in Figs. 4(b) and 4(e) for the generation of arbitrary superpositions of Fock states. In Figs. 15(a) and 15(b), we plot the discrete Fourier transform of the fields for generating the Fock states and the superpositions of Fock states, respectively. It can be seen from Fig. 15(a) that the field for generating Fock states only exists one peak in the frequency domain, regardless of the symmetry. While, many peaks exist for generating the superpositions of Fock states, leading to a significant broadening of the field spectrum, as seen from Fig. 15(b). We would like to mention that the frequency of the signal for generating target $|2\rangle$ is not twice as that for target $|1\rangle$, although the two states are one- and two-photon states. This is a result of the fact that the nonlinearity breaks the degeneracy of the oscillatory energy-level spacings. Below, we present a brief discussion on how to reduce the complexity of the waveform of the control field.

As shown above, the control fields $f_k(t)$ are designed based on the condition of $\dot{V}(t) \leq 0$, and it is clear that there are many cases that satisfy the inequality. This kind of feature provides us the possibility of designing much simpler fields. For instance, based on Eq. (7), the waveform of the control fields can be replaced by square pulses which satisfy the

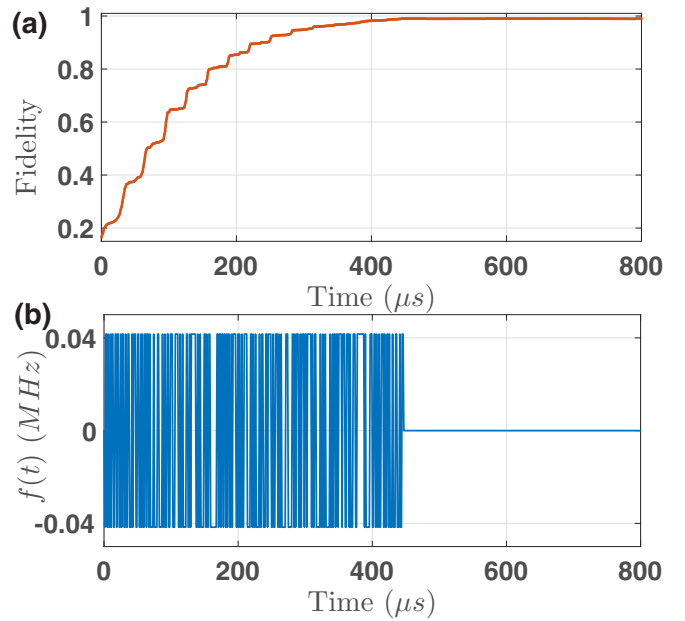


FIG. 16. (a) The fidelity $F_{T_2^R}$ and (b) The square pulse as a function of time. The initial state of the system is prepared in a coherent state $|\zeta_1\rangle$ and the final state is $|\zeta_2\rangle$ with $\zeta_1 = 0.5$ and $\zeta_2 = 1.85$. The other same parameters are: $\Omega = 2\pi \times 0.01$ MHz, $\omega_0 = \Omega$, $\omega = -2\Omega$, $\bar{n} = 0.0013$, $\gamma = 1/(10 \times 10^{-3})$ Hz, and $\chi = 2\pi \times 0.016$ MHz. The control field with square pulse are removed when the fidelity reaches 99%.

condition

$$f_k(t) = \begin{cases} F_k, & f_k(t) > 0 \\ 0, & f_k(t) = 0 \quad (k = 1, 2, \dots, K), \\ -F_k, & f_k(t) < 0 \end{cases} \quad (19)$$

where $F_k = \max |f_k(t)|$ is the maximum admissible strength of conventional control fields $f_k(t)$ in Eq. (7). This kind of bang-bang Lyapunov control ensures $\dot{V}(t) \leq 0$. The results for generating $|\zeta_2\rangle$ by using the bang-bang Lyapunov control with the real parameters are shown in Fig. 16. Again, we can achieve the target coherent state $|\zeta_2\rangle$ with the square pulse. In addition, we would like to point out that there are many other unconventional Lyapunov control techniques, such as the power-type and strength-type control laws [86], as well as the switching Lyapunov control law [87]. The square pulses in Eq. (19) belong to the strength-type control law, which has been widely used in experiments [88,89]. Compared to the waveform of the control field in Eq. (7), which varies at each moment, the amplitude of the square pulses remains unchanged. Thus, one can add a phase modulator to produce a π -phase difference in the control field and employ a waveform generator to make the value of the phase modulator meet the shape of square pulses.

V. CONCLUSION

In conclusion, we have proposed a scheme to generate various nonclassical states in nonlinear oscillator systems by using a state-based Lyapunov control. These nonclassical states are achieved by directly applying the customized external classical field to the nonlinear oscillator, which avoids

the requirement of interposing a nonlinear driving system to the resonator. We have shown that Fock states are achievable without precise time operation, while the generation of their superpositions requires a specific unitary transformation. The power of the scheme was demonstrated by numerically simulating the dynamics of the oscillator system and the Wigner functions of the oscillatory mode. The relatively larger energy gaps play an important role in the scheme, since the nonlinearity makes frequencies of transitions between adjacent oscillatory energy levels different, which is one of the prerequisite conditions of the scheme. The simulation results demonstrated that the scheme possesses the ability to generate the nonclassical states even in the presence of field fluctuation. In addition, we have shown that it is not necessary to prepare a perfect coherent state for the scheme. Moreover, the feasibility of the scheme with current experimental technology in super-

conducting systems has been discussed. To further simplify the realization of the scheme for other quantum systems, we have explored the possibility of replacing the control fields with square pulses. Thus, the scheme may offer an alternative way for the generation of nonclassical states in anharmonic oscillator systems.

ACKNOWLEDGMENTS

The authors acknowledge helpful discussions with C. S. Hu, B. H. Huang, and Y. H. Kang. This work is supported by the National Natural Science Foundation of China under Grants No. 11805036, No. 11575045, No. 11674060, and the Natural Science Foundation of Fujian Province of China under Grant No. 2018J01413.

-
- [1] V. Bužek and P. L. Knight, *Prog. Opt.* **34**, 1 (1995).
- [2] C. Bennett and G. Brassard, in *Proceedings of IEEE International Conference on Computers, Systems and Signal Processing* (Bangalore, India, 1984), pp. 175–179.
- [3] C. Liu, Z. Dutton, C. H. Behroozi, and L. V. Hau, *Nature* **409**, 490 (2001).
- [4] S. J. van Enk, J. I. Cirac, and P. Zoller, *Phys. Rev. Lett.* **79**, 5178 (1997); *Science* **279**, 205 (1998).
- [5] D. M. Meekhof, C. Monroe, B. E. King, W. M. Itano, and D. J. Wineland, *Phys. Rev. Lett.* **76**, 1796 (1996).
- [6] R. L. de Matos Filho and W. Vogel, *Phys. Rev. Lett.* **76**, 608 (1996); C. C. Gerry, *Phys. Rev. A* **55**, 2478 (1997); S. B. Zheng, *ibid.* **58**, 761 (1998).
- [7] A. Karimi, *Int. J. Theor. Phys.* **56**, 2703 (2017).
- [8] J. I. Cirac, A. S. Parkins, R. Blatt, and P. Zoller, *Phys. Rev. Lett.* **70**, 556 (1993).
- [9] B. Yurke, *Phys. Rev. A* **32**, 300 (1985).
- [10] C. M. Caves, K. S. Thorne, R. W. P. Drever, V. D. Sandberg, and M. Zimmermann, *Rev. Mod. Phys.* **52**, 341 (1980).
- [11] M. H. Michael, M. Silveri, R. T. Brierley, V. V. Albert, J. Salmilehto, L. Jiang, and S. M. Girvin, *Phys. Rev. X* **6**, 031006 (2016).
- [12] S. B. Zheng, *J. Opt. B: Quant. Semiclass. Opt.* **3**, 328 (2001).
- [13] Y. X. Liu, L. F. Wei, and F. Nori, *Europhys. Lett.* **67**, 941 (2004).
- [14] B. T. H. Varcoe, S. Brattke, and H. Walther, *New J. Phys.* **6**, 97 (2004).
- [15] F. O. Prado, W. Rosado, G. D. de Moraes Neto, and M. H. Y. Moussa, *Europhys. Lett.* **107**, 13001 (2014).
- [16] D. Kienzler, H. Y. Lo, B. Keitch, L. de Clercq, F. Leupold, F. Lindenfelser, M. Marinelli, V. Negnevitsky, and J. P. Home, *Science* **347**, 53 (2015).
- [17] S. B. Zheng and G. C. Guo, *Phys. Lett. A* **244**, 512 (1998).
- [18] A. T. Avelar and B. Baseia, *J. Opt. B: Quant. Semiclass. Opt.* **7**, 198 (2005).
- [19] P. Bertet, S. Osnaghi, P. Milman, A. Auffeves, P. Maioli, M. Brune, J. M. Raimond, and S. Haroche, *Phys. Rev. Lett.* **88**, 143601 (2002).
- [20] E. Waks, E. Dimanti, and Y. Yamamoto, *New J. Phys.* **8**, 4 (2006).
- [21] M. Hofheinz, E. M. Weig, M. Ansmann, R. C. Bialczak, E. Lucero, M. Neeley, A. D. O’Connell, H. Wang, J. M. Martinis, and A. N. Cleland, *Nature* **454**, 310 (2008).
- [22] M. Hofheinz, H. Wang, M. Ansmann, R. C. Bialczak, E. Lucero, M. Neeley, A. D. O’Connell, D. Sank, J. Wenner, J. M. Martinis, and A. N. Cleland, *Nature (London)* **459**, 546 (2009).
- [23] K. Vogel, V. M. Akulin, and W. P. Schleich, *Phys. Rev. Lett.* **71**, 1816 (1993).
- [24] C. K. Law and J. H. Eberly, *Phys. Rev. Lett.* **76**, 1055 (1996).
- [25] A. T. Avelar and B. Baseia, *Phys. Rev. A* **72**, 025801 (2005).
- [26] P. Liu, L. T. Shen, and Z. B. Yang, *Laser Phys. Lett.* **15**, 065206 (2018).
- [27] S. Deléglise, I. Dotsenko, C. Sayrin, J. Bernu, M. Brune, J. M. Raimond, and S. Haroche, *Nature (London)* **455**, 510 (2008).
- [28] F. Yoshihara, T. Fuse, S. Ashhab, K. Kakuyanagi, S. Saito, and K. Semba, *Nat. Phys.* **13**, 44 (2017).
- [29] S. Ashhab and F. Nori, *Phys. Rev. A* **81**, 042311 (2010).
- [30] M. A. Castellanos-Beltran, K. D. Irwin, G. C. Hilton, L. R. Vale, and K. W. Lehnert, *Nat. Phys.* **4**, 929 (2008).
- [31] G. Harel and G. Kurizki, *Phys. Rev. A* **54**, 5410 (1996).
- [32] B. M. Escher, A. T. Avelar, and B. Baseia, *Phys. Rev. A* **72**, 045803 (2005).
- [33] Q. Hou, W. Yang, M. Feng, and C. Chen, *JOSA B* **31**, 2671 (2014).
- [34] S. P. Premaratne, F. C. Wellstood, and B. S. Palmer, *Nat. Commun.* **8**, 14148 (2017).
- [35] W. Wang, L. Hu, Y. Xu, K. Liu, Y. Ma, S. B. Zheng, R. Vijay, Y. P. Song, L. M. Duan, and L. Sun, *Phys. Rev. Lett.* **118**, 223604 (2017).
- [36] T. V. Gevorgyan, A. R. Shahinyan, and G. Y. Kryuchkyan, *Phys. Rev. A* **85**, 053802 (2012).
- [37] R. Yanagimoto, E. Ng, T. Onodera, and H. Mabuchi, *Phys. Rev. A* **100**, 033822 (2019).
- [38] C. Shuang and K. Sen, *Acta Autom. Sin.* **33**, 28 (2007).
- [39] Y. Liu, S. Kuang, and S. Cong, *IEEE Trans. Cybern.* **47**, 3827 (2017).
- [40] S. Cong, *Control Theory Appl.* **29**, 273 (2012).
- [41] K. Beauchard, P. S. P. da Silva, and P. Rouchon, *Automatica* **48**, 68 (2012).

- [42] S. Kuang and S. Cong, *Acta Automat. Sinica* **36**, 1257 (2010).
- [43] Y. Pan, H. Amini, Z. Miao, J. Gough, V. Ugrinovskii, and M. R. James, *J. Math. Phys.* **55**, 062701 (2014).
- [44] S. Kuang and S. Cong, *Automatica* **44**, 98 (2008).
- [45] W. Cui and F. Nori, *Phys. Rev. A* **88**, 063823 (2013).
- [46] W. Li, C. Li, and H. Song, *Phys. Rev. E* **93**, 062221 (2016).
- [47] J. Hu, Q. Ke, and Y. Ji, *Int. J. Mod. Phys. B* **30**, 1650177 (2016).
- [48] M. Leib and M. J. Hartmann, *Phys. Rev. Lett.* **112**, 223603 (2014).
- [49] S. Cong, L. Hu, F. Yang, and J. Liu, *Acta Automat. Sinica* **39**, 360 (2013).
- [50] S. C. Hou, L. C. Wang, and X. X. Yi, *Phys. Lett. A* **378**, 699 (2014).
- [51] J. Wen and S. Cong, *Open Syst. Inf. Dyn.* **23**, 1650005 (2016).
- [52] N. Ghaeminezhad and S. Cong, *IEEE/CAA J. Autom. Sinica* **5**, 733 (2018).
- [53] X. X. Yi, X. L. Huang, C. Wu, and C. H. Oh, *Phys. Rev. A* **80**, 052316 (2009).
- [54] B. Xiong, X. Li, S. L. Chao, Z. Yang, W. Z. Zhang, W. Zhang, and L. Zhou, *Photonics Res.* **8**, 151 (2020).
- [55] S. C. Hou and X. X. Yi, *Quantum Info. Process.* **19**, 8 (2020).
- [56] T. V. Gevorgyan, A. R. Shahinyan, and G. Y. Kryuchkyan, *Phys. Rev. A* **79**, 053828 (2009).
- [57] A. Miranowicz, M. Paprzycka, Y. X. Liu, J. Bajer, and F. Nori, *Phys. Rev. A* **87**, 023809 (2013).
- [58] A. Miranowicz, J. Bajer, M. Paprzycka, Y. X. Liu, A. M. Zagoskin, and F. Nori, *Phys. Rev. A* **90**, 033831 (2014).
- [59] W. Leoński, S. Dyrting, and R. Tanaś, *J. Mod. Opt.* **44**, 2105 (1997).
- [60] A. Imamoglu, H. Schmidt, G. Woods, and M. Deutsch, *Phys. Rev. Lett.* **79**, 1467 (1997).
- [61] T. Rocheleau, T. Ndukum, C. Macklin, J. B. Hertzberg, A. A. Clerk, and K. C. Schwab, *Nature (London)* **463**, 72 (2010).
- [62] J. D. Teufel, T. Donner, L. Dale, J. H. Harlow, M. S. Allman, K. Cicak, A. J. Sirois, J. D. Whittaker, K. W. Lehnert, and R. W. Simmonds, *Nature (London)* **475**, 359 (2011).
- [63] X. Wang, S. Vinjanampathy, F. W. Strauch, and K. Jacobs, *Phys. Rev. Lett.* **107**, 177204 (2011).
- [64] H. W. Ch. Postma, I. Kozinsky, A. Hussian, and M. L. Roukes, *Appl. Phys. Lett.* **86**, 223105 (2005).
- [65] I. Kozinsky, H. W. Ch. Postma, O. Kogan, A. Husain, and M. L. Roukes, *Phys. Rev. Lett.* **99**, 207201 (2007).
- [66] P. D. Drummond and D. F. Walls, *J. Phys. A* **13**, 725 (1980).
- [67] L. Mandel and E. Wolf, *Optical Coherence and Quantum Optics*, Chap. 22 (Cambridge University Press, Cambridge, UK, 1995).
- [68] H. H. Adamyany, S. B. Manvelyan, and G. Y. Kryuchkyan, *Phys. Rev. A* **63**, 022102 (2001).
- [69] H. H. Adamyany, S. B. Manvelyan, and G. Yu. Kryuchkyan, *Phys. Rev. E* **64**, 046219 (2001).
- [70] G. Yu. Kryuchkyan and S. B. Manvelyan, *Phys. Rev. Lett.* **88**, 094101 (2002); *Phys. Rev. A* **68**, 013823 (2003).
- [71] J. La Salle and S. Lefschetz, *Stability by Lyapunov's Direct Method with Applications* (Academic Press, New York, 1961).
- [72] D. d'Alessandro, *Introduction to Quantum Control and Dynamics* (CRC Press, Boca Raton, FL, 2007).
- [73] D. Ran, W. J. Shan, Z. C. Shi, Z. B. Yang, J. Song, and Y. Xia, *Ann. Phys.* **396**, 44 (2018).
- [74] Z. C. Shi, X. L. Zhao, and X. X. Yi, *Phys. Rev. A* **91**, 032301 (2015).
- [75] C. Shuang, *Control of Quantum Systems: Theory and Methods* (Wiley, New York, 2014).
- [76] Y. X. Zeng, T. Gebremariam, M. S. Ding, and C. Li, *JOSA B* **35**, 2334 (2018).
- [77] W. P. Schleich, *Quantum Optics in Phase Space* (Wiley, Berlin, 2001).
- [78] S. M. Barnett and P. M. Radmore, *Methods in Theoretical Quantum Optics* (Cambridge University Press, Cambridge, UK, 1997).
- [79] M. O. Scully and M. S. Zubairy, *Quantum Optics* (Cambridge University Press, Cambridge, UK, 1999).
- [80] W. Leon-acutecki, *Phys. Rev. A* **55**, 3874 (1997).
- [81] Y. Xu, Y. Ma, W. Cai, X. Mu, W. Dai, W. Wang, L. Hu, X. Li, J. Han, H. Wang, Y. P. Song, Z.-B. Yang, S.-B. Zheng, and L. Sun, *Phys. Rev. Lett.* **124**, 120501 (2020).
- [82] C. Deng, J. L. Orgiazzi, F. Shen, S. Ashhab, and A. Lupascu, *Phys. Rev. Lett.* **115**, 133601 (2015).
- [83] W. Ning, X. J. Huang, P. R. Han, H. Li, H. Deng, Z. B. Yang, Z. R. Zhong, Y. Xia, K. Xu, D. Zheng, and S. B. Zheng, *Phys. Rev. Lett.* **123**, 060502 (2019).
- [84] Z. B. Yang, P. R. Han, X. J. Huang, W. Ning, H. Li, K. Xu, D. Zheng, H. Fan, S. B. Zheng, [arXiv:1909.03170v2](https://arxiv.org/abs/1909.03170v2).
- [85] Y. Ma, Y. Xu, X. Mu, W. Cai, L. Hu, W. Wang, X. Pan, H. Wang, Y. P. Song, C.-L. Zou, and L. Sun, *Nat. Phys.* **16**, 827 (2020).
- [86] S. C. Hou, M. A. Khan, X. X. Yi, D. Dong, and Ian R. Petersen, *Phys. Rev. A* **86**, 022321 (2012).
- [87] S. Kuang, D. Y. Dong, and Ian R. Petersen, *Automatica* **81**, 164 (2017).
- [88] F. Schmidt-Kaler, H. Häffner, M. Riebe, S. Gulde, G. P. T. Lancaster, T. Deuschle, C. Becher, C. F. Roos, J. Eschne, and R. Blatt, *Nature* **422**, 408 (2003).
- [89] J. J. Morton, A. M. Tyryshkin, A. Ardavan, S. C. Benjamin, K. Porfyraakis, S. A. Lyon, and G. A. D. Briggs, *Nat. Phys.* **2**, 40 (2006).